NMR Studies of 4-^{19}F-Phenylalanine-Labeled Intestinal Fatty Acid Binding Protein: Evidence for Conformational Heterogeneity in the Native State†

Hua Li and Carl Frieden*

Department of Biochemistry and Molecular Biophysics, Box 8231, Washington University School of Medicine, 660 South Euclid Avenue, St. Louis, Missouri 63110

Received November 12, 2004; Revised Manuscript Received December 7, 2004

ABSTRACT: ^{19}F-Nuclear magnetic resonance (NMR) studies have been carried out after incorporation of 4-^{19}F-phenylalanine into the intestinal fatty acid binding protein (IFABP), a protein composed of two β-sheets containing a large hydrophobic cavity into which ligands bind. NMR spectra have been obtained with both the ligand-free and ligand-bound (oleate) forms. There are 29 residues involved in van der Waals or hydrophobic interactions or both to form a U-shaped ligand binding pocket (Sacchettni J. C., Scapin G., Gopaul D., and Gordon J. I. (1992) *J. Biol. Chem. 267*, 23534−23545). The protein contains eight phenylalanines, and all are included in those residues that line the pocket. Peak assignments were made using site-specific incorporation of 4-^{19}F-phenylalanine. Fluorine is a highly sensitive probe to monitor the conformation and dynamics of the side chains in native state. We find that chemical exchange in the binding pocket exists in the native apo- and holo-state. Of the eight phenylalanine residues, Phe2, Phe47, Phe62, Phe68, and Phe93 are arranged on one side of the binding pocket, and all exist in two conformations with Phe2, Phe47, and Phe62 showing exchange cross-peaks with minor conformation in ^{19}F−^{19}F nuclear Overhauser effect (NOESY) spectra. The line widths of Phe68 and Phe93 are broader than those of other phenylalanine residues and can be deconvoluted into two peaks. Phe47, Phe62, Phe68, Phe93, and Trp82 have been proposed to be involved in the early stage of collapse (Ropson, I. J., and Frieden, C. (1992) *Proc. Natl. Acad. Sci U.S.A. 89*, 7222−7226), but a temperature study suggests that Phe47 behaves differently than other residues and may be more involved in a later stage of folding, for example, side chain stabilization. In the holo-form, Phe17 shows an extra exchange cross-peak in addition to those exchange cross-peaks observed in apo-form. Holo-IFABP exhibits broader line width than the apo-form, suggesting more flexibility of the binding cavity upon ligand binding.

The intestinal fatty acid binding protein (IFABP)[1] is a member of a class of proteins of similar structure that bind fatty acids, restinoids and bile salts. Crystal structures of the apo (*1*) and holo (*2*) IFABP as well as the NMR structures for the apo (*3*) and holo form (*4*) have been solved. The protein consists of two β-sheets surrounding a large interior cavity into which the ligand binds. A small helical region may serve as a portal for the ligand. NMR studies have also probed the dynamics of IFABP (*5*) as well as other members of the family (*6*) for both apo- and holo-forms. Additionally, molecular dynamics simulations have been carried out to study the dynamic processes (*7*−*9*). Most of those residues that exhibit conformational exchanges are within the portal region, which has been shown to be more flexible. Only a few of those that showed backbone conformational exchange arise from residues that line the binding cavity (*10*).

There are always some discrepancies between crystal and NMR structure and dynamics revealed by simulations and NMR relaxation studies. Those discrepancies mainly arise from the lack of full description of side chains. Thus, it is not unexpected that the bulk of violations between simulated data and experimental NOE involve side chain atoms (*9*).

^{19}F NMR spectroscopy is unique in probing structural and dynamic features of the side chains of proteins. Despite its high electronegativity and the strength of carbon−fluorine dipole, the incorporation of fluorine, which has similar size as proton, into amino acids, primarily aromatic amino acids, appears to have a minimal effect on a variety of systems in terms of function and structure (*11*−*15*). Additionally, ^{19}F NMR is extremely sensitive to environmental changes and shows a very wide dispersion of chemical shifts making it easier to apply line shape or line width analysis (*11*, *12*).

In a previous study of IFABP, 6-^{19}F-tryptophan was incorporated (*11*) to study the mechanism of protein folding. These studies led to the observation of an intermediate in the folding pathway that included several residues in and near the D−E turn (see Figure 1). There are, however, only two tryptophan residues in IFABP and there are several reasons to characterize the eight phenylalanine residues in detail. As shown in Figure 1 these residues are distributed throughout the protein. Phe2 is located at the N-terminal regions while Phe17, Phe47, Phe62, Phe68, Phe93 and Phe128 are located in the α1, βC, βD, βE, βG, βJ strands, respectively. Phe55 is located in the turn between the βC and βD strands. In the crystal structure of holo-IFABP (*2*), aromatic side chains cluster in two regions. A U-shaped

† This work supported by NIH Grant DK13332.

* Corresponding author. Phone: (314) 362-3344. Fax: (314) 362−7183. E-mail: frieden@biochem.wustl.edu.

[1] Abbreviations: IFABP, intestinal fatty acid binding protein; EDTA, ethylenediamine tetracetic acid; NOESY, nuclear Overhauser effect spectroscopy; holo-, ligand bound; apo-, ligand free.

10.1021/bi047600l CCC: $30.25
Published on Web 01/28/2005

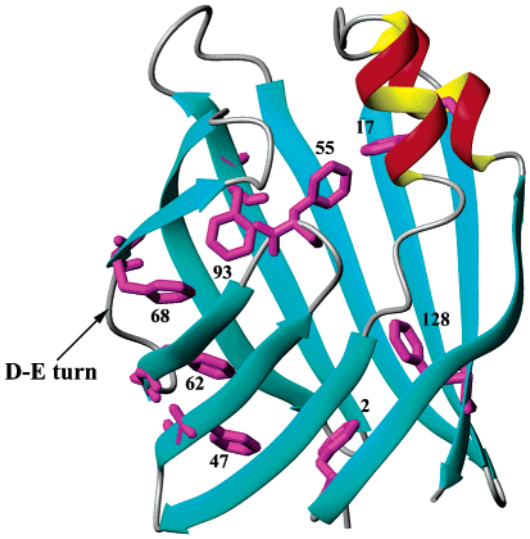

FIGURE 1: The crystal structure (PDB entry: 1IFB) of apo-IFABP (*2*) showing the location of eight phenylalanine residues. The diagram was prepared using MolMol (*35*).

arrangement consists of Phe47, Phe62, Trp82, Phe68, Trp6, Phe2, and Phe93, located near the carboxylate group of the bound fatty acid, while Tyr14, Phe17, Tyr117 and Tyr119 are close to the end of the methylene chain of bound fatty acid with the methyl group of fatty acid pointing toward Phe55. Each phenylalanine may play a role in the structure.

^{15}N NMR relaxation and ^{1}H exchange has been used to indirectly probe the dynamics of the binding cavity (*16*). Other methods used to probe the cavity dynamics include measurements of magnetic relaxation dispersion (MRD) (*17*) and internal water simulations (*9*). ^{19}F NMR provides an alternative means to probe the dynamics (side chain dynamics) of the cavity with and without ligand through line shape and line width analysis.

MATERIALS AND METHODS

Chemicals. 4-^{19}F-Phe was obtained from ACROS Organics (New Jersey). Oleic acid and heptane were from Sigma-Aldrich. All other chemicals were reagent grade.

Incorporation of Eight 4-^{19}F-Phenylalanines into IFABP. The production of 4-^{19}F-labeled phenylalanine IFABP using an *Escherichia coli* bacterial expression system was essentially as described by Frieden et al. (*14*). More than 90% labeling, as indicated by mass spectroscopy, was achieved by using the phenylalanine auxotroph DL 39 containing the plasmid pQE80 IFABP in defined medium with 0.1 mM unlabeled phenylalanine at 37 °C. After growing cells to an A_{600} of 3, they were harvested and resuspended in a defined medium containing 0.2 mM 4-^{19}F-phenlylalanine. After 30 min, IFABP production was induced with 1 mM isopropyl β-D-thiogalactoside (IPTG) for 3 h before harvesting again. The protein was purified as outlined by Kim et al. (*18*).

Site-Specific Labeling of IFABP. The initial assignment of 4-^{19}F-Phe resonances in IFABP was achieved by site-specific labeling as established by Furter (*19*) and modified by Bann et al. (*13*). Similar to the expression of PapD (*14*), plasmid pRO117 contains tRNA Phe/amber gene and plasmid pQE 80 contains yeast tRNA synthetase and IFABP gene. The strain K10−F6Δ was used for the transformation of these two plasmids. The cells were first grown in medium containing 0.2 mM unlabeled phenlylalanine to an A_{600} of 1, harvested and then resuspended in medium containing 0.04 mM unlabled phenylalanine and 3 mM 4-^{19}F-phenylalanine. The protein was induced with 1 mM IPTG 30 min later and purified the same way as for fully ^{19}F-Phe labeled IFABP.

To solve the ambiguous assignment of Phe47 and Phe93, two mutants, each containing two 4-^{19}F-Phe residues, were made, one labeled in position Phe47 and Phe68, the other labeled in position Phe68 and Phe93. They were expressed as described above. All proteins were essentially purified and delipidated as described previously (*18*).

NMR Sample Preparation. For 1D spectra, the samples were made by dilution of a 2.4 mM stock solution into 20 mM potassium phosphate buffer containing 0.25 mM EDTA at pH 7.3 to give a final concentration of 200 μM protein.

Holo-IFABP was prepared by mixing 2.4 mM (about 1 mL) stock apo-IFABP with 10 μL oleic acid/heptane solution (1:2 ratio in volume), gently shaken for 1 min and then centrifuged at 13k rpm for 5 min. The partition coefficient of oleic acid in heptane and water is $10^{5.36}$, and the solubility of heptane in water is 0.0003%, much lower than other solvents (i.e., ethanol) involved in the preparation of holo-IFABP (*20*). Heptane had no effect on the NMR spectrum of IFABP. We also prepared the holo-protein solution by diluting the protein and oleic acid to ~2 μM and then concentrated to about ~200 μM by Amicon ultrafiltration with a YM-10 membrane. The NMR spectrum is also identical to that prepared in the presence of a heptane solution of oleic acid. An advantage of using heptane is that any excess oleate partitions into the heptane phase, thus excluding the formation of micelles in the protein solution.

^{19}F NMR Spectroscopy. ^{19}F NMR spectra were acquired on a Varian Unity-Plus 500 MHz spectrometer operating at 470.3 MHz with a Varian Cryo-Q dedicated to 5 mm ^{19}F probe. The ^{19}F probe was cooled and kept at 20 °K with the Varian Cryo-Q open cycle Cryogenic system. Unless otherwise indicated, all 1D spectra were recorded at 20 °C with 64 scans and processed by NMRPipe (*21*) with 12 Hz exponential line broadening. The chemical exchange rate was determined by performing phase-sensitive 2D-NOESY experiments at different mixing times (50 ms to 200ms) (*22*, *23*). The 2D data were analyzed by the Pipp program (*24*). The spectra were referenced to an internal standard of 6-fluro-tryptophan (~0.2mM, the actual chemical shift is −46.293 ppm relative to TFA), and all samples contained 8% (vol/vol) D_2O. No correction to pH was made with D_2O in the sample.

RESULTS

Assignment of ^{19}F Resonances in Apo-IFABP. The location of the eight phenylalanines in the structure of apo-IFABP is shown in Figure 1. Incorporation of 4-^{19}F-Phe into IFABP gives rise to eight well-resolved ^{19}F resonances (Figure 2). The stability of the fluorine labeled IFABP is essentially identical to that of the unlabeled protein as indicated by urea denaturation data (not shown), suggesting incorporation of fluorine does not change the protein stability. The initial assignment of the eight resonances was achieved by site-directed incorporation of 4-^{19}F-Phe as described in Methods. When using singly labeled protein to make these assignments, two phenomena were observed which made the assignment

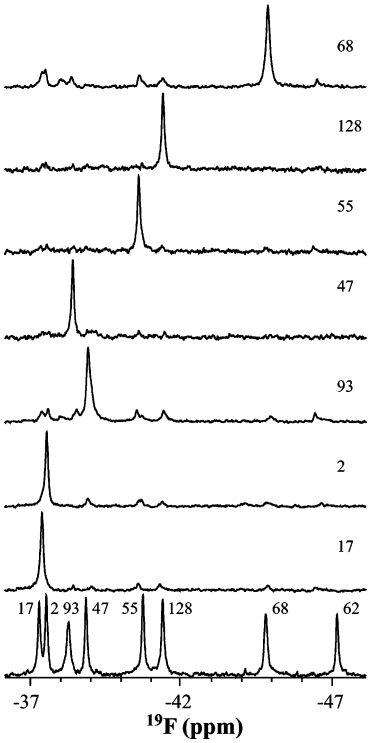

FIGURE 2: ^{19}F NMR spectra of 4-^{19}F-Phe labeled IFABP. The resonances were assigned by site-specific incorporation of 4-^{19}F-labeled phenylalanine. The spectra were acquired at 20 °C with 64 scans and processed with 12 Hz exponential line broadening. The sample condition is 0.2 mM protein in 20 mM potassium phosphate buffer containing 0.25 mM EDTA, 10% D_2O, pH 7.3.

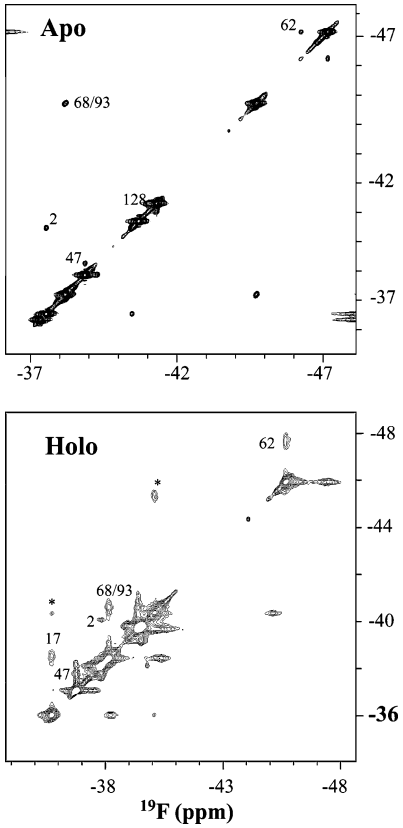

FIGURE 3: 2D-NOESY spectra of apo- and holo-IFABP in 20 mM potassium phosphate buffer containing 0.25 mM EDTA at pH 7.3. The protein concentration used was 1 mM. The spectra were acquired with 32 scans with 100 points on F1 dimension. The mixing time was 200 ms. In the apo-form, Phe68 and Phe93 shows NOE cross-peak, Phe2, Phe47, Phe62 and Phe128 show exchange cross-peaks. In the holo-form, Phe68 and Phe93 also shows NOE cross-peak, and Phe2, Phe17, Phe47 and Phe62 exhibit exchange cross-peaks. The two peaks marked with an asterisk (*) cannot be unambiguously assigned.

ambiguous. First, the ^{19}F resonances of single labeling were not quite aligned with those in the spectrum of full labeling, possibly due to the extreme sensitivity of ^{19}F to local environment. Second, from 3% to 7% of every Phe position incorporated 4-^{19}F-Phe, the so-called "contamination" as mentioned by Furter (*19*). In the NMR spectra, the contamination is manifested by the appearance of minor ^{19}F NMR peaks, which are actually helpful for the assignment. From the proximity of chemical shift and minor peaks due to contamination, it would appear that peaks at −38.84 ppm and −38.26 ppm should be assigned to Phe93 and Phe47, respectively. However, the peak at −38.26 ppm shows an NOE cross-peak with Phe68 (Figure 3, Apo). After adding hydrogens using InsightII (Accelrys, CA) to the crystal structure of apo-IFABP (PDB entry: 1IFB), the distance between 4-H−Phe68 and 4-H−Phe93 is found to be 2.05 Å, while that between 4-H−Phe68 and 4-H−Phe47 is 11.5 Å. To resolve the assignment ambiguity, two doubly labeled mutants were made, one labeled at Phe47 and Phe68 and the other at Phe93 and Phe68. Only the latter (Figure 4B) showed an NOE cross-peak while the former (Figure 4A) did not. Therefore the peaks at −38.84 ppm and −38.26 ppm were assigned to Phe47 and Phe93, respectively. The possible reason for the ambiguity in this assignment is that Phe93 and Phe47 are located in the pocket surrounded by several aromatic side chains. Any slight change of any of those aromatic side chains may cause a ring current effect, which is a major contribution to chemical shift changes. Thus, when two peaks are close, one must be careful about the assignments. The assignment of the peaks of Phe17 and Phe2, which are close in Figure 2, was confirmed by the exchange cross-peak of Phe2 in both native and acidic conditions (Figure 4C and 4D).

In the 2D-NOESY spectrum of apo-IFABP at native condition (20 mM potassium phosphate buffer containing 0.25 mM EDTA at pH 7.3) (Figure 3), an exchange cross-peak was observed for Phe2 from mixing times of 50 ms to 200 ms, thus excluding the possibility of spin diffusion from surrounding hydrogens. When the pH of apo-IFABP is decreased to 2.8, the exchange cross-peak became stronger as the population of the minor conformation increased (data not shown). This assignment is further confirmed by a 2D-NOESY experiment using singly 4-^{19}F-Phe2 labeled IFABP (Figure 4C). To rule out the possibility of labeling contamination, the pH of the protein solution with singly ^{19}F-labeling on Phe2 was decreased to pH 2.8 too. The exchange cross-peak became stronger at low pH with the population of the upfield conformation increased (Figure 4D), strongly supporting that the cross-peak observed for Phe2 is due to chemical exchange.

*Comparison of Apo- and Holo-IFABP***.** From the 2D-NOESY spectra of apo- and holo-IFABP (oleate-IFABP complex) (Figure 3), it would appear that the holo-IFABP is more heterogeneous than apo-IFABP as indicted by more cross-peaks. In both forms, Phe68 and Phe93 show cross-peaks as a consequence of their close proximity. In the apo-

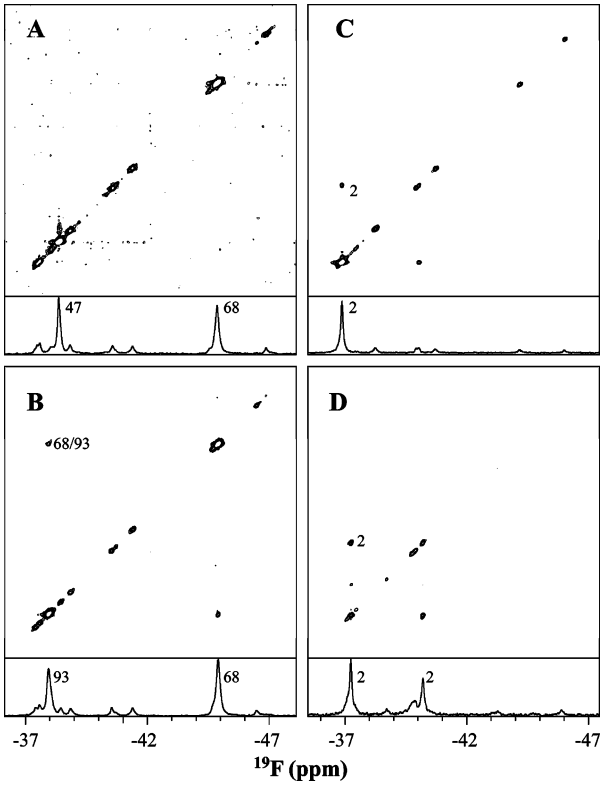

FIGURE 4: 2D-NOESY spectra used to solve assignment ambiguity. The mixing time was set to 200 ms with 100 points in F1 dimension. (A) 4-^{19}F-labeling on Phe47 and Phe68. The protein concentration is between 2.5 and 3 mM and 56 scans were used. No NOE cross-peak was observed between Phe47 and Phe68. (B) 4-^{19}F-labeling on Phe68 and Phe93. The protein concentration was 1 mM and 24 scans was used. Phe68 and Phe93 show a clear NOE cross-peak. (C) The assignment of Phe2 was confirmed by the exchange cross-peak at pH 7.3. (D) The exchange cross-peak of Phe2 at pH 2.8. The protein concentration used was about 1 mM and 32 scans were used to record the data.

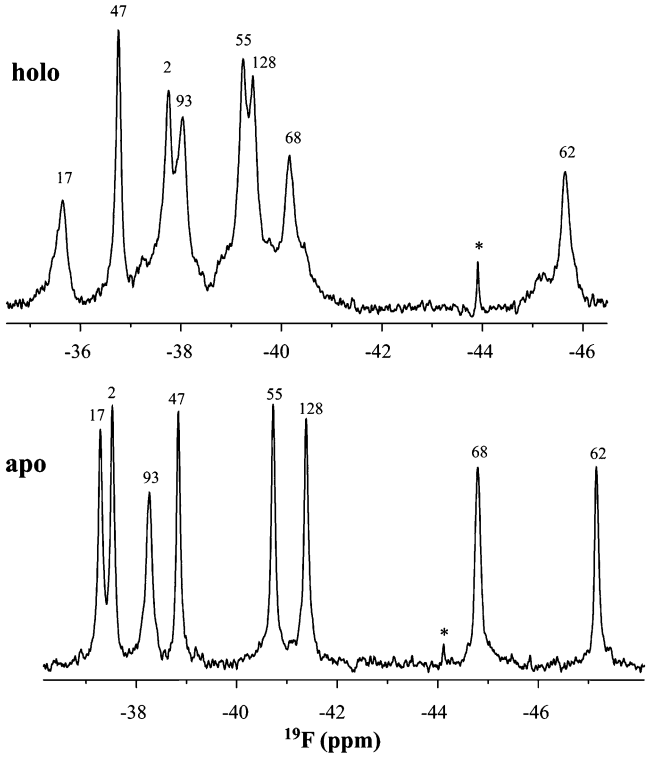

FIGURE 5: Spectrum comparison of apo- and holo-IFABP (oleate-IFABP complex) in 20 mM potassium phosphate buffer containing 0.25 mM EDTA at pH 7.3. The protein concentration was 200 μM. The spectra were recorded with 64 scans and processed with 12 Hz exponential line broadening. The spectra were referenced to 6-^{19}F-tryptophan (the actual chemical shift is −46.293 ppm relative to TFA). Resonances marked with an asterisk (*) at ∼ −44 ppm in both spectra are artifacts.

form, Phe2, Phe47, Phe62 and Phe128 exhibit exchange cross-peaks. In the holo-form, in addition to the exchange cross-peaks of Phe2, Phe47 and Phe62, three additional cross-peaks appear with one being assigned to the exchange cross-peak of Phe17 (Figure 3). The other two peaks cannot be unambiguously assigned.

Figure 5 shows the 1D spectra of apo- and holo-IFABP under native conditions. The chemical shift difference between the apo- and holo-IFABP are shown in Table 1. All ^{19}F labeled-Phe (except Phe2) resonances were shifted downfield. The line widths of holo-form are much broader than those in the apo-form for all phenylalanines except Phe47, which did not change upon ligand binding (Table 1).

Side Chain Dynamics in the Native Protein. As it is close to the C-terminus, the behavior of Phe2 in apo-IFABP might be expected to act more like a free amino acid or one in random coil region with resonance around −40.2 ppm, a region where free ^{19}F-Phe resonates. Only about 8% population resonated at −40.5 ppm with the other peak resonating downfield (∼ −37.3 ppm). These two resonances represent two conformations which are in slow exchange (Figure 4C) with a rate estimated to be 3.6 ± 1.6 s^{-1}, obtained from 2D-NOESY experiments performed at different mixing times (*22*). With increasing urea, there is no evidence that the relative population of Phe2 at −40.5 ppm grows faster than other denatured resonances (Li and Frieden, unpublished data). This phenomenon may indicate that the side chain of Phe2 of IFABP is structured and well correlated with other residues even in high urea concentrations.

Under native conditions (20 mM potassium phosphate buffer containing 0.25 mM EDTA at pH 7.3), there are also at least two conformations for Phe62 in apo-IFABP, with chemical shifts at −46.24 ppm and −47.15 ppm, respectively, in slow exchange as indicated by their exchange cross-peak (Figure 3, Apo), although the downfield peak only accounts for ∼0.1% to ∼0.5% total intensity. The chemical shift difference of these two conformations is about 428 Hz and the exchange rate was estimated to be 10.8 ± 3.3 s^{-1} by taking the population ratio as 0.2:99.8. Phe47 also exhibits two conformations shown by exchange cross-peaks in NOESY (Figure 3, Apo). However, the minor conformation at upfield only accounts for a population of <0.5%. Minor conformations exist for both Phe47 and Phe62. Since the hydrophobic pocket formed by Phe47, Phe62, Phe68, Phe93, Trp82 and two leucines at positions 64 and 89, we postulate that some conformation heterogeneity might occur for other side chains in this region. In the spectra obtained for doubly labeled ^{19}F-Phe at Phe68 and Phe93, we observed two conformations for Phe68, further confirmed by temperature dependence of the NMR spectrum.

Effects of Temperature. Since protein structure and function are temperature dependent, the influence of temperature on NMR spectra is either through dynamics or through shifting a temperature-dependent equilibrium. The parameters

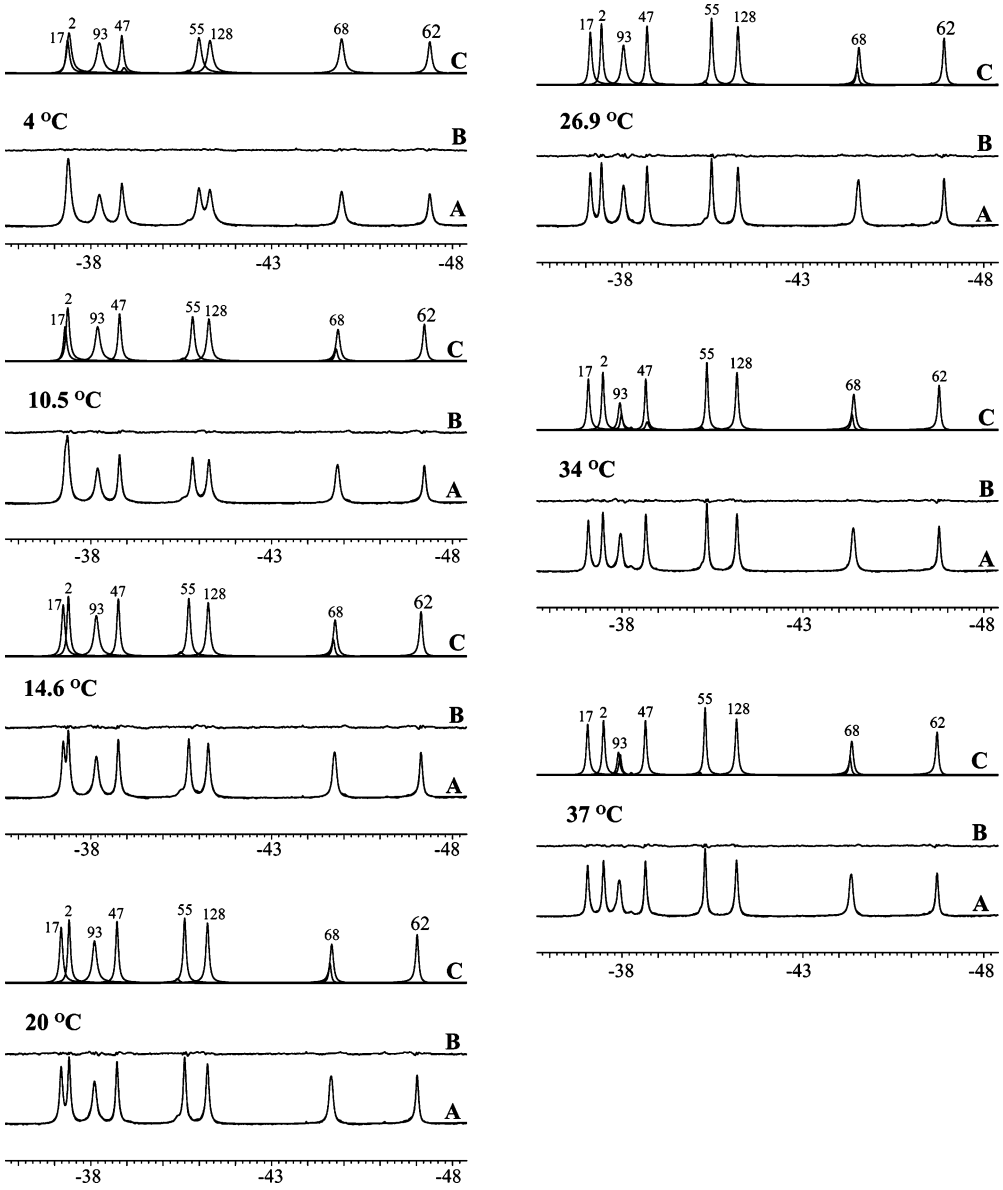

FIGURE 6: The spectra deconvoluted by Bayesian analysis at different temperatures. At each temperature, three spectra are shown, with (A) being the overlay of real spectrum and deconvoluted spectrum, (B) residual spectrum from real spectrum and deconvoluted spectrum and (C) deconvoluted spectrum.

Table 1: Chemical Shift (δ) and Line Width (LW) Difference of 4-^{19}F-Phe between Apo- and Holo-Form IFABP

	residue number							
	2	17	47	55	62	68	93	128
δ_{apo} (ppm)	−37.52	−37.29	−38.84	−40.72	−47.16	−44.80	−38.26	−41.38
δ_{holo} (ppm)	−37.75	−35.65	−36.76	−39.24	−45.65	−40.16	−38.04	−39.43
$\Delta\delta_{holo-apo}$ (ppm)	−0.23	1.64	2.08	1.48	1.51	4.64	0.22	1.95
LW_{apo} (Hz)	41.7	48.8	42.8	44.1	45.5	64.7	69.9	48.3
LW_{holo} (Hz)	80.1	90.8	42.4	75.8	93.0	94.7	98.4	81.3

that reflect this influence are relaxation times, line widths and chemical shifts. Temperature-dependent relaxation studies have been used to probe motions on multiple time scales (*25*) and the interactions between protein and DNA (*26*). The combined use of temperature dependent changes in the chemical shift of backbone amide protons with H/D exchange rates has been shown to be a far more reliable indicator of hydrogen bonding than either alone (*27*). The NMR line width is proportional to the apparent relaxation rate, R_2*, which is the sum of spin−spin relaxation rate, R_2, and the rate from other factors. Usually, slow conformational fluctuations in a protein contribute an exchange rate (R_{ex}) to R_2*, resulting in line broadening. Temperature-dependent line width analysis has been used to probe side chain dynamics of molten globule state of α-lactalbumin by ^{19}F NMR (*12*) and temperature dependent ^{15}N-transverse relaxation has been used for the identification of exchange heterogeneity for the folding and unfolding studies of protein GB1 (*28*).

The NMR spectra of apo-IFABP were obtained at 4 °C, 10.5 °C, 14.6 °C, 20 °C, 26.9 °C, 34 °C, 37 °C and shown in Figure 6. The spectra were processed with 10 Hz exponential line broadening and deconvoluted by Bayesian

analysis (*29*) with maximum resonance set between 10 and 20 for each spectrum. The results are independent of the setting of maximum resonances. At each temperature, A (in Figure 6) is the superposition of real spectrum and deconvoluted spectrum, B is the residual spectrum of real spectrum and deconvoluted spectrum and C is the deconvoluted spectrum. At temperatures higher than 10 °C, the broad resonance of Phe68 was always deconvoluted into two resonances (spectra labeled C) with about a ~1:3.5 to ~1:2.6 ratio for the downfield conformation relative to the upfield conformation (Figure 6). The chemical shift difference of the two conformations is about 25 Hz, less than the line width of both conformations, which could explain the lack of exchange cross-peak in 2D-NOESY between these two conformations. The deconvolution of Phe68 into two separate peaks indicates that they could exchange slowly at a rate less than 25 s^{-1}, their chemical shift difference. When the chemical shift difference of these two conformations increased as condition changes (e.g. low pH), these two conformations showed an exchange cross-peak (Li and Frieden, in preparation). There is no significant difference in the ratio and chemical shift difference for these two conformations with temperature. Although the line width of the two conformations is different their temperature dependence of chemical shifts for these two conformations is almost the same.

The broadest peak of Phe93 separated into two peaks above 30 °C with the ratio of the two conformations (downfield:upfield) increasing from ~1:2.2 at 34 °C to ~1:1.2 at 37 °C (Figure 6). The chemical shift difference of these two conformations is also about 25 Hz. The changing ratio of these two conformations with temperature could possibly explain why the broadest peak of Phe93 was not separated into two peaks by Bayesian analysis at temperature lower than 34 °C. Since temperature shifts the equilibrium of these two conformations, the ratio of the two conformations could be very small at low temperatures, which makes it impossible to deconvolute this peak. This is the case for Phe62. Although from the 2D-NOESY, an exchange peak is very obvious for two conformations at a ratio between 0.1:99.9 and 0.5:99.5, Bayesian analysis did not show the peak of a minor conformation due to its very weak intensity.

DISCUSSION

Comparison between Apo- and Holo-IFABP. The dramatic downfield chemical shift change for most phenylalanines upon ligand binding is mainly due to a deshielding effect. In the apo-form, the binding site contains 13 ordered water molecules, the so-called "water pump" (*30*). Because of the higher electronegativity of oxygen atoms than that of carbons, this "water pump" imposes a higher shielding effect on side chains in the binding pocket. The binding of oleic acid is accompanied by the exclusion of some of those ordered water molecules (*2*, *30*), resulting in a deshielding effect on the side chains surrounding oleate. Of the seven downfield shifted phenylalanines, Phe68 was shifted the most and Phe93 was shifted the least. In the crystal structure of apo-IFABP (*30*), Phe68 is somewhat closer to the ordered water molecules than other phenylalanines (Figure 7A). But in the holo-IFABP binding with oleate, two carbon atoms of oleate are within 4.5 Å range contact to Phe93 while no carbon atom are within 4.5 Å of Phe68 (*10*). As in a similar structure

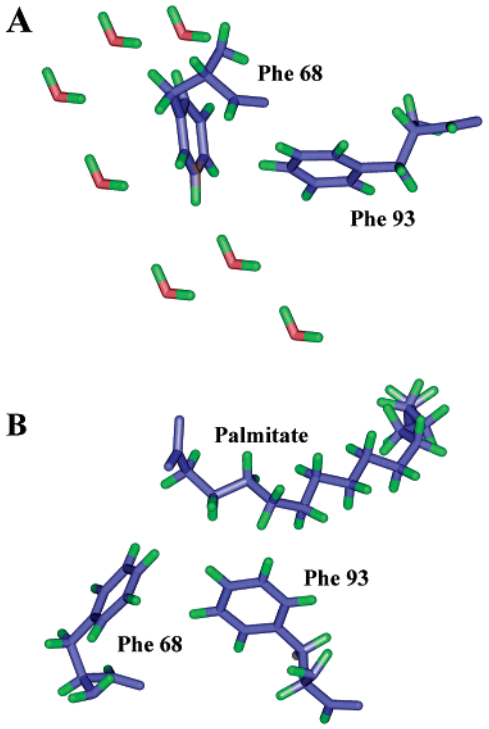

FIGURE 7: (A) Diagram of Phe68 and Phe93 to surrounding water molecules in apo-IFABP (PDB entry; 1IFB). (B) Diagram of Phe68 and Phe93 to bound palmitate (PDB entry 2IFB).

with palmitate (*2*), 4 carbon atoms of palmitate were in contact with Phe93 within 4.5 Å range and only one carbon atom is within 4.5 Å to Phe68 (Figure 7B). Therefore, Phe93 experiences more shielding effect from the fatty acid chain than Phe68. In other words, Phe93 experiences less of an overall deshielding effect than does Phe68. The small upfield shift of Phe2 could be caused by slight conformational perturbation, which is consistent with the observation that the largest difference between C_α positions of holo- and apo-IFABP exists in the first three N-terminus residues (*30*).

Cistola and co-workers (*4*, *16*) have shown that holo-IFABP exhibited sharper peaks than the apo-form and the backbone of the holo-form was more ordered than the apo-form. Unlike that observed by Hodsdon and Cistola (*16*), however, most of the side chains of phenylalanines of holo-IFABP showed broader line widths than those of the apo-form (Table 1). One possible explanation is due to on−off exchange of ligand. As the binding affinity of oleate-IFABP is between 20 and 40 nM and the oleate left in the solution is saturated by heptane (~5 μM), >99% protein is in the holo-form. Hence, the exchange of ligand between apo- and holo-form is very slow and unlikely to cause line broadening. The most likely explanation for line broadening is the presence of more motion in the binding cavity with the side chains becoming more disordered upon ligand binding. As the binding of fatty acid is maintained by the interaction between the backbone of the fatty acid and side chains in the binding cavity, side chain flexibility may be reflected by the mobility of fatty acid. This logic is supported by simulated data (*9*), which show that palmitate retains substantial flexibility in the protein cavity with considerable overall motion. Although the time scale as manifested by line broadening is out of the reach of molecular dynamics simulations, the simulation data mentioned above are still

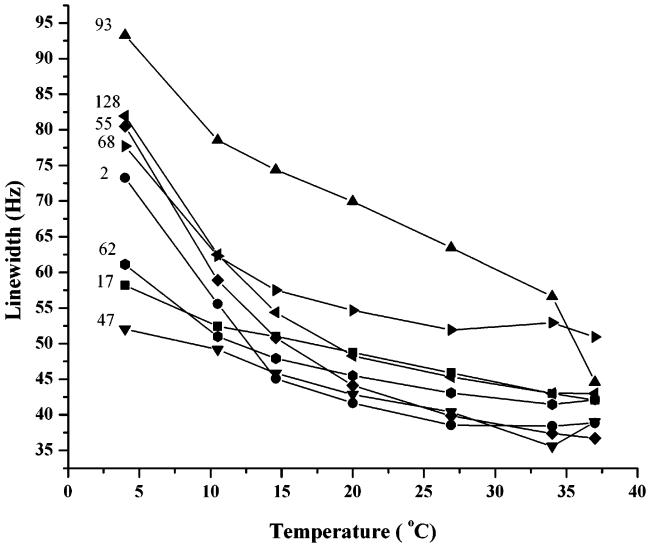

FIGURE 8: The line width of eight 4-^{19}F-labeled phenylalanines in IFABP as a function of temperature. The protein concentration was 1 mM in 20 mM potassium phosphate buffer containing 0.25 mM EDTA (pH 7.3). The sharp decrease of the line width of Phe93 from 34 °C to 37 °C was due to the fact the Phe93 resonance was deconvoluted into two peaks. The data shown here for Phe93 at 34 °C to 37 °C is the line width of the major downfield conformation.

expected to provide some insights about the dynamics of the cavity at slower time scales as motions at different time scales are always coupled to some extent (*9*). The simulations (*9*) also revealed the following properties: 1) there is less similarity between side chain hydrogen bond networks of apo-and holo-form than between their backbone counterparts, indicating the overall mobility of side chains; 2) holo-IFABP shows a higher rate of exchange between internal and external water molecules than apo-IFABP even though smaller amount of water molecules reside in the cavity of holo-IFABP. Therefore, it is the dynamics of the fatty acid in the cavity that leads to the extra motions of side chains, resulting in line broadening. Of the eight phenylalanines, only Phe47 maintains the same line width upon ligand binding as in the apo-form (Table 1), indicating that the fatty acid is less influential to Phe47 than other phenylalanines.

It should be emphasized that higher ordering of backbone of the holo-form, as suggested by Cistola and co-workers (*4*, *16*), does not conflict with more flexibility of the side chains because the ordering of backbone can counteract the disorder effect of side chains. This explains the general observation that holo-IFABP is more stable than apo-IFABP even though the side chains of holo-IFABP are more flexible.

Side Chain Dynamics. Figure 8 shows that the line widths decrease with the increasing temperature for all of the ^{19}F-labeled phenylalanines, suggesting additional motional processes at elevated temperatures. We interpret those additional motions to be in the fast exchange category since R_{ex} increases with temperature in the slow exchange regime and decreases in the fast exchange regime (*28*). As Phe2 and Phe128 are located near the N- and C-teminus of the protein, respectively, and Phe55 is located in the turn between βC and βD strands and believed to be disordered (*30*), we would expect narrower line width due to higher degree of freedom of these side chains relative to others. Yet, for IFABP, this is not the case. At 4 °C, Phe2, Phe55 and Phe128 have broader line widths than do Phe17, Phe47 and Phe62. (The discussion of Phe68 and Phe93 is described below). This implies that Phe2, Phe55 and Phe128 are structured with extensive low rate motions. With increasing temperature, the line widths of Phe2, Phe55 and Phe128 sharpen faster than those of Phe17, Phe47 and Phe62. At 10 °C or above, they have essentially the same line width and the same temperature dependence, further indicating that, even at higher temperature, Phe2, Phe55 and Phe128 do not show obvious a higher degree of motion freedom.

The chemical exchange with minor conformation for Phe2, Phe47 and Phe62 was observed for both apo- and holo-IFABP, which may suggest that these exchanges between major and minor conformations are an inherent property of IFABP. The extra exchange cross-peak of Phe17 in holo-form could be the result of its extensive contact with oleate, as the region that fatty acid bends upon binding with IFABP is very close to Phe17. Structural perturbation (i.e. lower pH) may further characterize the conformational exchange of Phe17.

Implications for the Line-Broadening of Phe68 and Phe93. While both Phe68 and Phe93 show only a single NMR peak, these peaks are broader than other resonances. There could be two reasons. First, there may be two or more conformation forms in intermediate to fast exchange at a rate comparable to their chemical shift difference. Second, they may be in slow exchange, but the chemical shift difference is smaller than the line width, which makes direct observation of exchange cross-peak impossible. The latter reason applies to Phe68 and Phe93 as shown in the results. The persistence of the two conformations of Phe68 at different temperatures may be a hint of its special function as a barrier, together with Phe62 and Phe47, between the interior and exterior of the protein (*31*). This barrier could open and close through side chain rotations, at a rate which is comparable to estimated exchange rate, allowing for such events as water entering/exiting and coordinating ligand binding. Alanine mutations of each phenylalanines (except Phe2 and Phe128) reduce the binding affinity of the protein with F68A showing largest reduction of binding affinity among a large number of mutants which were examined (*31*). This observation further explains the exchange property of Phe68 as residues or regions, which are critical for function, are always dynamic.

It has been shown that the mere observation of a single exchange broadened resonance does not necessarily mean that the exchange is fast on the chemical shift time scale (*32*). This statement is further discussed by Palmer et al. (*33*) for two conformations (A and B) in slow exchange. In the slow exchange limit, the resonance at frequency Ω_B of conformation B is lower in intensity than the resonance at frequency Ω_A of conformation A by a factor of p_B/p_A (where p_B/p_A is the population ratio of conformation B and conformation A), and broader by a factor of $(R^0_{2B} + p_A k_{ex})/(R^0_{2A} + p_B k_{ex})$, where the R^0_{2A} and R^0_{2B} are relaxation decay constants and k_{ex} is the exchange rate. Therefore, in the case of $p_A \gg p_B$, the resonance (Ω_B) of conformation B may not be detectable (*33*, *34*). The broadened peak of Phe93 could be the result of slow exchange also, with the minor conformation broadened. Another reason to classify Phe93 in the slow exchange limit is that it forms a hydrophobic cluster with Phe68, Phe62 and Trp82 (*11*), which were identified to be

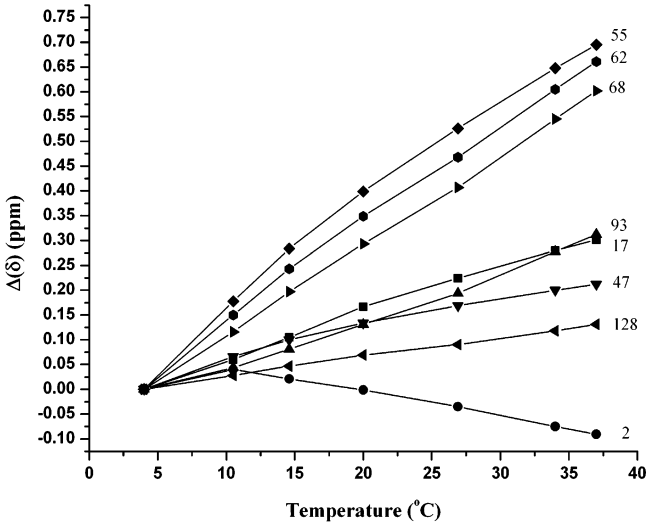

FIGURE 9: Chemical shift change as a function of temperature (temperature coefficient) for apo-IFABP. The conditions are the same as described in Figure 8.

in slow exchange. Hence the motion of Phe93 at a quite different frequency is less likely.

Unusual Behavior of Phe47 in the Hydrophobic Core. In the model proposed by Ropson and Frieden (*11*), a hydrophobic cluster is comprised of Trp82, Phe47, Phe62, Phe68, Phe93 and two leucine residues, with each aromatic amino acid on a different strand of the β-sheet. In the structure (*30*) Phe47, Phe62, Phe68, partially stack on each other, with average distance ~6 Å between Phe47 and Phe62, and ~ 5.5 Å between Phe62 and Phe68. Ropson and Frieden (*11*) observed chemical exchange phenomena of Trp82 in this most hydrophobic region. In this study, we found that chemical exchange is prevalent in this region. All four phenylanalines involved in this region are in low-frequency exchange.

The present study suggests, however, that it may not be appropriate to include Phe47 in the hydrophobic core. There are several lines to support this suggestion. First, Phe47 has the narrowest line width over almost the whole experimental temperature range, indicating higher degree of motional freedom for Phe47 relative to other phenylalanines. Second, Phe47 experienced the smallest chemical shift change during the course of urea denaturation, possibly due to its independence on overall conformational perturbation (Li and Frieden, data not shown). Third, its temperature coefficient of the chemical shift is the smallest, only higher than those of Phe2 and Phe128, which are close to the C-teminus and N-terminus, respectively, while the temperature coefficients are the largest for Phe62 and Phe68 (Figure 9). These results imply that with the increasing temperature, Phe47 moves independently of Phe62 and Phe68. Fourth, binding of oleate did not change the line width of Phe47 (Table 1). There are at least two reasons for grouping Trp82, Phe62, Phe68 and Phe93 together. First, they are all in slow chemical exchange. Second, their chemical shifts change in the same upfield direction while that of Phe47 slightly changes downfield at low urea concentration (1.5 M urea) but moves upfield at high urea concentration (Li and Frieden, data not shown). This suggests that Phe47 and other aromatic residues are in different frames of motion and the hydrophobic collapse during early folding stage may not include the side chain of Phe47. The exchange phenomenon of Phe47 at 20 °C or lower could be the result of the exchange of Phe62 or even Phe68. As Phe68, Phe62 and Phe47 partially stack on each other (Figure 1), the conformational change of Phe62 (i.e. rotation of aromatic ring) may sterically or energetically unfavorable for Phe47, which will make Phe47 change its conformation (i.e. rotation of side chain) coordinately. In this case, Phe47 could be involved in a later stage of folding, i.e., side chain stabilization.

In summary, ^{19}F NMR is a powerful tool for characterizing local side chain structural and dynamical properties of a protein. The data obtained are complementary to crystallographic and structural NMR studies. Furthermore, ^{19}F NMR can examine either individual side chain or a group of side chains to determine whether motions are concerted or not. For IFABP the surprising result is that motion of side chains in the binding cavity is greater in the holo-form compared to the apo protein while the backbone is less flexible in the holo-form (*3*).

ACKNOWLEDGMENT

The authors would like to thank Drs. D. P. Cistola and M. E. Hodsdon for helpful discussions and Robert Horton for excellent technical assistance.

REFERENCES

1. Scapin, G., Gordon, J. I., and Sacchettini, J. C. (1992) Refinement of the structure of recombinant rat intestinal fatty acid-binding apoprotein at 1.2-A resolution, *J. Biol. Chem. 267*, 4253−4269.
2. Sacchettini, J. C., Gordon, J. I., and Banaszak, L. J. (1989) Crystal structure of rat intestinal fatty-acid-binding protein. Refinement and analysis of the *Escherichia coli*-derived protein with bound palmitate, *J. Mol. Biol. 208*, 327−339.
3. Hodsdon, M. E., and Cistola, D. P. (1997) Discrete Backbone Disorder In the Nuclear Magnetic Resonance Structure Of Apo Intestinal Fatty Acid-Binding Protein − Implications For the Mechanism Of Ligand Entry, *Biochemistry 36*, 1450−1460.
4. Hodsdon, M. E., Ponder, J. W., and Cistola, D. P. (1996) The NMR Solution Structure Of Intestinal Fatty Acid-Binding Protein Complexed With Palmitate − Application Of a Novel Distance Geometry Algorithm, *J. Mol. Biol. 264*, 585−602.
5. Zhu, L., Kurian, E., Prendergast, F. G., and Kemple, M. D. (1999) Dynamics of palmitic acid complexed with rat intestinal fatty acid binding protein, *Biochemistry 38*, 1554−1561.
6. Lu, J., Lin, C. L., Tang, C., Ponder, J. W., Kao, J. L., Cistola, D. P., and Li, E. (1999) The structure and dynamics of rat apo-cellular retinol-binding protein II in solution: comparison with the X-ray structure, *J. Mol. Biol. 286*, 1179−1195.
7. Woolf, T. B., Grossfield, A., and Tychko, M. (2000) Differences between apo and three holo forms of the intestinal fatty acid binding protein seen by molecular dynamics computer calculations, *Biophys. J. 78*, 608−625.
8. Likic, V. A., and Prendergast, F. G. (1999) Structure and dynamics of the fatty acid binding cavity in apo rat intestinal fatty acid binding protein, *Protein Sci. 8*, 1649−1657.
9. Bakowies, D., and van Gunsteren, W. F. (2002) Simulations of apo and holo-fatty acid binding protein: structure and dynamics of protein, ligand and internal water, *J. Mol. Biol. 315*, 713−736.
10. Sacchettini, J. C., Scapin, G., Gopaul, D., and Gordon, J. I. (1992) Refinement of the structure of escherichia-coli-derived rat intestinal fatty-acid binding-protein with bound oleate to 1.75-angstrom resolution − correlation with the structures of the apoprotein and the protein with bound palmitate, *J. Biol. Chem. 267*, 23534−23545.
11. Ropson, I. J., and Frieden, C. (1992) Dynamic NMR spectral analysis and protein folding: identification of a highly populated folding intermediate of rat intestinal fatty acid-binding protein by ^{19}F NMR, *Proc. Natl. Acad. Sci. U.S.A. 89*, 7222−7226.

12. Bai, P., Luo, L., and Peng, Z. (2000) Side chain accessibility and dynamics in the molten globule state of alpha-lactalbumin: a ^{19}F NMR study, *Biochemistry 39*, 372−380.
13. Bann, J. G., and Frieden, C. (2004) Folding and Domain-Domain Interactions of the Chaperone PapD Measured by ^{19}F NMR, *Biochemistry 43*, 13775−13786.
14. Frieden, C., Hoeltzli, S. D., and Bann, J. G. (2004) The preparation of ^{19}F-labeled proteins for NMR studies, *Methods Enzymol. 380*, 400−415.
15. Grage, S. L., Wang, J., Cross, T. A., and Ulrich, A. S. (2002) Solid-state ^{19}F NMR analysis of ^{19}F-labeled tryptophan in gramicidin A in oriented membranes, *Biophys. J. 83*, 3336−3350.
16. Hodsdon, M. E., and Cistola, D. P. (1997) Ligand Binding Alters the Backbone Mobility Of Intestinal Fatty Acid-Binding Protein As Monitored By N-15 NMR Relaxation and H-1 Exchange, *Biochemistry 36*, 2278−2290.
17. Wiesner, S., Kurian, E., Prendergast, F. G., and Halle, B. (1999) Water molecules in the binding cavity of intestinal fatty acid binding protein: dynamic characterization by water 17O and 2H magnetic relaxation dispersion, *J. Mol. Biol. 286*, 233−246.
18. Kim, K., Ramanathan, R., and Frieden, C. (1997) Intestinal Fatty Acid Binding Protein − a Specific Residue In One Turn Appears to Stabilize the Native Structure and Be Responsible For Slow Refolding, *Protein Sci. 6*, 364−372.
19. Furter, R. (1998) Expansion of the genetic code: site-directed p-fluoro-phenylalanine incorporation in *Escherichia coli*, *Protein Sci. 7*, 419−426.
20. Arighi, C. N., Rossi, J. P., and Delfino, J. M. (1998) Temperature-induced conformational transition of intestinal fatty acid binding protein enhancing ligand binding: a functional, spectroscopic, and molecular modeling study, *Biochemistry 37*, 16802−16814.
21. Delaglio, F., Grzesiek, S., Vuister, G. W., Zhu, G., Pfeifer, J., and Bax, A. (1995) NMRPipe: a multidimensional spectral processing system based on UNIX pipes, *J. Biomol. NMR. 6*, 277−293.
22. Jeener, J., Meier, B. H., Bachmann, P. L., and Ernst, R. R. (1979) Investigation of exchange processes by two-dimensional NMR spectroscopy, *J. Chem. Phys. 71*, 4546−4553.
23. Perrin, C. L., and Dwyer, T. J. (1990) Application of two-dimensional NMR to kinetics of chemical exchange, *Chem. Rev. 90*, 935−967.
24. Garrett, D. S., Powers, R., Gronenborn, A. M., and Clore, G. M. (1991) A common sense approach to peak picking two-, three- and four-dimensional spectra using automatic computer analysis of contour diagrams, *J. Magn. Reson. 95*, 214−220.
25. Mandel, A. M., Akke, M., and Palmer, A. G., 3rd. (1996) Dynamics of ribonuclease H: temperature dependence of motions on multiple time scales, *Biochemistry 35*, 16009−16023.
26. Bracken, C., Carr, P. A., Cavanagh, J., and Palmer, A. G., 3rd. (1999) Temperature dependence of intramolecular dynamics of the basic leucine zipper of GCN4: implications for the entropy of association with DNA, *J. Mol. Biol. 285*, 2133−2146.
27. Baxter, N. J., and Williamson, M. P. (1997) Temperature dependence of 1H chemical shifts in proteins, *J. Biomol. NMR 9*, 359−369.
28. Ding, K., Louis, J. M., and Gronenborn, A. M. (2004) Insights into conformation and dynamics of protein GB1 during folding and unfolding by NMR, *J. Mol. Biol. 335*, 1299−1307.
29. Bretthorst, G. L. (1990) Bayesian Analysis. I. Parameter estimation using quadrature NMR models, *J. Magn. Reson. 88*, 533−551.
30. Sacchettini, J. C., Gordon, J. I., and Banaszak, L. J. (1989) Refined apoprotein structure of rat intestinal fatty acid binding protein produced in *Escherichia coli*, *Proc. Natl. Acad. Sci. U.S.A. 86*, 7736−7740.
31. Richieri, G. V., Low, P. J., Ogata, R. T., and Kleinfeld, A. M. (1997) Mutants of rat intestinal fatty acid-binding protein illustrate the critical role played by enthalpy−entropy compensation in ligand binding, *J. Biol. Chem. 272*, 16737−16740.
32. Ishima, R., and Torchia, D. A. (1999) Estimating the time scale of chemical exchange of proteins from measurements of transverse relaxation rates in solution, *J. Biomol. NMR 14*, 369−372.
33. Palmer, A. G., 3rd, Kroenke, C. D., and Loria, J. P. (2001) Nuclear magnetic resonance methods for quantifying microsecond-to-millisecond motions in biological macromolecules, *Methods Enzymol. 339*, 204−238.
34. Woessner, D. E. (1996) Brownian motion and its effect in NMR chemical exchange and relaxation in liquids, *Concepts Magn. Reson. 8*, 397−421.
35. Koradi, R., Billeter, M., and Wuthrich, K. (1996) MOLMOL: a program for display and analysis of macromolecular structures, *J. Mol. Graphics 14*, 51−55.

BI047600L